Polymer Chemistry

The Role of Side-chain Branch Position on Thermal Property of Poly-3-alkylthiophenes

Journal:	*Polymer Chemistry*
Manuscript ID	PY-ART-07-2019-001026.R2
Article Type:	Paper
Date Submitted by the Author:	02-Oct-2019
Complete List of Authors:	Gu, Xiaodan; University of Southern Mississippi, School of Polymer Science and Engineering Cao, Zhiqiang; University of Southern Mississippi, School of Polymer Science and Engineering Galuska, Luke; University of Southern Mississippi, School of Polymer Science and Engineering Qian, Zhiyuan; University of Southern Mississippi, School of Polymer Science and Engineering Zhang, Song; University of Southern Mississippi, School of Polymer Science and Engineering Huang, Lifeng; University of Southern Mississippi, School of Polymers and High Performance Materials Prine, Nathaniel; University of Southern Mississippi, School of Polymer Science and Engineering Li, Tianyu; Oak Ridge National Laboratory; University of Tennessee Knoxville He, Youjun; Oak Ridge National Laboratory Hong, Kunlun; Oak Ridge National Laboratory, Center for Nanophase Materials Science; Oak Ridge National Laboratory, Center for Nanophase Materials Science

ARTICLE

The Role of Side-chain Branch Position on Thermal Property of Poly-3-alkylthiophenes

Received 00th January 20xx,
Accepted 00th January 20xx

DOI: 10.1039/x0xx00000x

Zhiqiang Cao,[a] Luke Galuska,[a] Zhiyuan Qian,[a] Song Zhang, [a] Lifeng Huang,[a] Nathaniel Prine,[a] Tianyu Li,[b, c] Youjun He,[b] Kunlun Hong,*[b, c] and Xiaodan Gu*[a]

Thermomechanical properties of conjugated polymers (CPs) are greatly influenced by both their microstructures and backbone structures. In the present work, to investigate the effect of side-chain branch position on the backbone's mobility and molecular packing structure, four poly (3-alkylthiophene-2, 5-diyl) derivatives (P3ATs) with different side chains, either branched and linear, were synthesized by a quasi-living Kumada catalyst transfer polymerization (KCTP) method. The side-chain branch position greatly influences the glass transition temperature (T_g) of the backbone of P3ATs as well as the melting temperature (T_m), as measured by dynamical mechanical analysis (DMA) and differential scanning calorimetry (DSC) respectively. Placing the branching point closer to the conjugated backbone leads to increased backbone T_g and T_m. Also, according to grazing incidence wide-angle X-ray scattering (GIWAXS) results, branching closer to the backbone causes tighter packing in side-chain direction. The tighter packing along with side-chain direction coresponds with higher T_m, which decreases the free volume of the polymer system and subsequently increases the T_g at the same time. This work provided the first in-depth understanding of branch point influence on thermal properties of poly-3-alkylthiophenes. It would provide guidance to the future development of side-chain engineering on next-generation CPs with desirable thermomechnical property for stretchable and wearable electronics.

Introduction

Scientific interest in developing conjugated polymers (CPs) for future plastic electronics has rapidly increased over recent years due to their solution processability, tunable optical and electronic properties, and broad bio-compatibility.[1–4] Significant technological milestones have been achieved such as photovoltaic efficiencies exceeding 16% efficiency[5,6], carrier mobilities approaching those of state-of-the-art inorganic semiconductors (e.g., metal oxides) and polycrystalline silicon[7,8], and a new generation of technologies[9] that were previously unimaginable.

Generally, CPs contain two parts: π-conjugated backbones with delocalized π-bonds, which are directly responsible for the charge transport and optoelectronic properties, and peripheral flexible side chains, which are critical to their synthesis and processing because of generally enhanced solubilities.[10] Recently, there are growing amounts of evidence that side chains not only just improve solubilities and solution processabilities[11], but also impact many physical properties of CPs, including molecular packing[12–17], dynamics of backbones[18], and charge transport[3–5,7–12]. The side chains of CPs could have several direct impacts on the CPs, including tuning molecular packing by steric hindrance effect and backbone dynamic due to the plasticization effect on the rigid backbones which determine thermomechanical properties of conjugated polymers.

The thermal transition temperatures are critical parameters to tune the thermal stability, elastic modulus, and deformability of conjugated polymers.[23–25] T_g of CPs plays a key role in the thermal stability of donor:acceptor semiconductor blends for organic solar cells.[24] Also, the increase in the T_g of CPs increases its elastic modulus[25]. Furthermore, viscoelastic behavior of CPs is prevalent when polymer backbone poses sub-ambient T_g.[26] Longer alkyl side chains lower the backbone glass transition temperature (T_g) and melting temperature (T_m) as exemplified by the P3ATs with linear alkyl side chains.[18,23,27,28] It is reported that unsubstituted polythiophene presents a T_g of ~120 °C,[27] and when increasing linear alkyl side-chain length (0-8 carbons), T_g drops significantly, i.e., poly(3-butylthiophene) (P3BT) shows a T_g of 45 °C, followed by 12 °C for poly(3-hexylthiophene) (P3HT) and −13 °C for poly(3-octylthiophene) (P3OT).[29] Meanwhile, the main chain melting transitions for P3BT occurs at 243 °C[30], as the number of alkyl groups in the side chain increases from 4 to 12, the melting

[a] School of Polymer Science and Engineering, Center for Optoelectronic Materials and Devices, The University of Southern Mississippi, Hattiesburg, MS 39406, USA.
[b] Center for Nanophase Materials Sciences, Oak Ridge National Laboratory, Oak Ridge, Tennessee 37831, United States.
[c] Department of Materials Science and Engineering and Chemical & Biomolecular Engineering, University of Tennessee, Knoxville, Tennessee 37996, United States.
Electronic Supplementary Information (ESI) available: [details of any supplementary information available should be included here]. See DOI: 10.1039/x0xx00000x

transition subsequently decreases to 234 °C for P3HT[31], 190 °C for P3OT[30], 155 °C for poly(3-dodecylthiophene) (P3DDT)[30].

Compared to linear alkyl chains, branched isomers impart stronger steric hindrance effect thus result in better solubility. Therefore, branched alkyl chains are widely introduced in donor-acceptor type CPs.[15,25,32–38] Take the diketopyrrolopyrrole (DPP) based polymers for example, it is the close intermolecular packing distance, which arises from the dipolar fused lactam carbonyl units and planarity of the thiophene flanking units, necessitated that long and branched alkyl side chains on both nitrogen pyrrole groups are commonly attached to improve polymer solubility.[32,33] Also, branched alkyl chains with adjustable branching positions have been recently reported.[14,21,34,39] Moving the branching position of side chains away from the backbone has been shown to result in shorter π–π stacking distances and thus higher charge carrier mobility.[14,21] Similar works were performed on other CPs for the effect of branched side chain position on the microstructure and electronic property.[34,39] However, how these different branched alkyl isomers affect the thermal property in conjugated polymers (e.g., backbone T_g and T_m) is still not fully understood.

In this work, we aim to address the question raised above. We picked P3AT systems due to easy synthesis by metal-catalyzed chain transfer polymerizations. This method allows us to obtain narrowly dispersed polymers so that we can minimize or even rule out the potential effect of dispersity on polymer's thermal property. Herein, we designed and synthesized four P3AT polymers with systematically varied side-chain branch locations, and their chemical structures are shown in **Scheme 1**. P3HT was chosen as the reference polymer and the methyl group was shifted along the side chain. The thermal transitions and molecular packing were investigated using DMA, DSC, and GIWAXS. Results showed that the branch position greatly influences the T_g and T_m of P3ATs. The T_m and T_g changed as much as 36 °C and 60 °C respectively, simply by tuning the branch location. It should be emphasized that a better understanding of the importance of side-chain engineering will have larger implications in fine-tuning of the backbone T_g to create soft and deformable conjugated polymers which opens new route to make flexible and stretchable electronic devices or to make thin glassy film for enhanced device stability at elevated operation temperature.

Experimental

Materials

Anhydrous tetrahydrofuran (THF) was purchased from VWR International Co. and used without further purification. Methanol, magnesium, N-bromosuccinimide (NBS), chloroform, acetic acid, 3-bromothiophene, 1,3-[bis(diphenylphosphino)propane]dichloronickel(II) ($Ni(dppp)Cl_2$), 1-bromopentane, 1-bromohexane, 1-bromo-4-methylpentane, 1-bromo-3-methylpentane, isopropylmagnesium chloride solution and 2,2,6,6-Tetramethylpiperidinylmagnesium chloride lithium chloride complex solution were purchased from Aldrich Chemical Co. and used without further purification. All reactions were performed under nitrogen, using oven-dried glassware.

Synthesis of P3AT polymers

Polymers were synthesized by a quasi-living Kumada catalyst transfer polymerization (KCTP) method as reported previously.[40–45] The synthetic route was shown in **Scheme 2**. Typically, in an inert gas environment, 3-bromothiophene and alkyl magnesium bromide participated in a Kumuda reaction with $Ni(dppp)Cl_2$ as the catalyst to yield 3-alkylthiophene compounds. After bromiding in 2 position by reacting with NBS in a mixture solvent of chloroform and acetic acid, 2-bromo-3-alkythiophene monomers were obtained. Then, 2-bromo-3-alkylthiophenes reacted with Grignard reagent (2, 2, 6, 6-tetramethylpiperidinylmagnesium chloride lithium chloride complex solution) to form 2-bromo-5-magnesiumchloridelithiumchloride-3-alkylthiophenes. Finally, using $Ni(dppp)Cl_2$ as the catalyst, the monomers were polymerized to form various P3AT polymers. After the synthesis, the samples were precipitated in cold methanol and purified via Soxhlet extraction with methanol, to afford the product. These polymers have a high regularity of over 97%.

Size Exclusion Chromatography (SEC)

A SEC system with an Agilent 1310B 1260 Infinity Isocratic HPLC pump equipped with a multiangle static light scattering detector with a 664 nm laser (DAWN HELEOS-II, Wyatt) and a refractive index (RI) detector with a 658 nm laser (Optilab T-rEX, Wyatt) was used to determine the molecular weight of the synthesized P3ATs. This system contains four Phenomenex Phenogel columns in series. THF was the eluent with a flow rate of 1 mL/min. Polystyrene standards were used to ascertain the dispersity values.

Nuclear Magnetic Resonance (NMR)

^{1}H-NMR and ^{13}C-NMR spectra were measured on a Varian-500 MHz NMR spectrometer. Chemical shifts were reported in ppm relative to $CDCl_3$ at 7.27 ppm and 77.23 ppm for ^{1}H-NMR and ^{13}C-NMR respectively.

Dynamical Mechanical Analysis (DMA)

DMA measurements were performed on a TA Q800 DMA by a modified DMA method.[46] Samples were prepared by drop-casting of polymer solutions on top of a glass fiber mesh.The backbone T_g was determined to be the temperature corresponding to the peak of tan δ and loss modulus (E") for all samples. The DMA measurements were performed in strain-controlled mode. Temperature ramp experiments were performed at a temperature range of −110 to 300 °C and a heating rate of 3 °C/min with a fixed frequency of 1 Hz. The strain imposed was in the linear regime.

Differential Scanning Calorimetry (DSC)

DSC measurements were performed with Mettler-Toledo DSC3+ and Q-2000 DSC (TA Instruments). The samples were first heated above the melting temperature followed by

cooling to -90 °C with a heating rate of 10 °C/min. After that, the samples were reheated up at the same rate. The DSC data were taken at the second reheating scan for data analysis to remove thermal history.

Grazing Incidence Wide-Angle X-ray Scattering (GIWAXS)

GIWAXS measurements were performed on beamline 11-3 at the Stanford Synchrotron Radiation Lightsource (SSRL). Data was collected under a helium environment with an incident beam energy of 12.7 keV and an incidence angle of 0.12°. The samples for this measurement were prepared on bare Si substrates via spin casting at 2k rpm for two minutes at the following concentrations: 12, 15, 15, and 10 mg/ml in anhydrous chlorobenzene for P3PT, P3HT, P3(4MP)T, and P3(3MP)T respectively. Each sample underwent a five-minute exposure and the scattering data was collected with a two-dimensional Rayonix MX225 CCD area detector at a sample to detector distance of about 200 mm. The scattering data analysis was performed using Nika software package for Wavemetrics Igor Pro, in combination with WAXS tools.[47]

Atomic Force Microscope (AFM)

Images were acquired on Asylum S AFM Microscope in AC-air mode. The samples were casted on the flat silicon substrate as described above. Films were spun-coat from a 12 mg mL^{-1} chlorobenzene solution onto silicon substrates at 2000 rpm, following by thermal annealing at 130 °C for 30 min inside a N_2-filled glove box.

UV-Vis-NIR spectroscopy

UV-Vis-NIR spectra were measured by a Cary 5000 UV-Vis-NIR spectrophotometer. Solution absorption data was acquired from chlorobenzene solution. For thin film absorption, films were spun-coat from a 10 mg mL^{-1} chlorobenzene solution onto quartz substrates at 2000 rpm, following by thermal annealing at 130 °C for 30 min inside a N_2-filled glove box.

Organic Field Effect Transistor (OFET)

Organic field-effect transistors were fabricated in the bottom-gate top-contact configuration. Heavily doped n-type Si substrates served as the gate electrodes, and a 300-nm thick thermally grown silicon dioxide overlayer was used as the dielectric layer. P3AT films were spin-coated from 12 mg/ml chlorobenzene solution and annealed under a nitrogen atmosphere at 130 °C for 1 hour and allowed to cool naturally. The source and drain electrodes were patterned using standard shadow masking within a metal evaporator to deposit 40 nm thick gold electrodes with a channel width and length of 100 and 50 μm respectively. The electrical measurements of the OFET devices were carried out with a Keithley 4200 semiconductor parameter analyzer within a glove box under a nitrogen atmosphere. Device performance, such as mobility, on/off ratio, and threshold voltage, were obtained from transfer plots with OFET devices operating in the saturation regime at a constant source-drain voltage of -100 V and sweeping the gate voltage from 20 to -100 V. Mobility values were specifically taken as the slope of $I_{D,sat}^{1/2}$ vs V_G plot from -10 to -60 V for conservative measurement.

Results and discussion

Molecular characterization

Four different P3AT polymers were synthesized by a quasi-living Kumada catalyst transfer polymerization (KCTP) method according to previous reports (see experimental section). The molecular weight and polydispersity were characterized by SEC in THF at 35 °C. **Table 1** summarized the material's molecular weights and polydispersities of four P3AT polymers. All four P3ATs have similar molecular weights, thus the potential influence of molecular weight on T_g is ruled out. ^{1}H NMR and ^{13}C NMR spectroscopy were utilized to confirm these P3AT polymers (Figure S1~S8). According to ^{1}H NMR spectra (**Figure 1**), the chemical structure of the side chains can be determined. For the polymers with linear side chains (P3PT and P3HT), there is only one methyl group at the end of the side chains which is confirmed by a triple peak at 0.9 ~1.0 ppm. Polymers with branched side chains, namely P3(4MP)T and P3(3MP)T, contain two methyl groups in the side chains, which is verified by the intensity increases for the peaks at 0.9 ~1.0 ppm. Furthermore, due to two methyl groups in the side chains of P3(4MP)T are attached to the same carbon, a double peak at 0.9 ~1.0 ppm was observed. However, two methyl groups in the side chains of P3(3MP)T are attached to two different carbons, so a triple peak at 0.88 ~0.96 ppm is shown to correspond to the terminal methyl group and a double peak at 0.96 ~1.04 ascribes to the inside methyl group. Besides, as a result of the chirality of the branching side-chain structure of P3(3MP)T, split peaks were found.

The optical properties of P3ATs in both chlorobenzene solutions and solid-state thin films were investigated by UV-Vis spectroscopy, as shown in **Figure 2** and **Figure S9**. The result shows that the polymers in dilute chlorobenzene solutions adopt random coil geometries with semiflexible backbones.[48–51] All polymers have similar absorption spectra with a maximum centered ~ 460 nm. From solutions to solid films, this peak of the absorption spectra is red-shifted to 540 nm to 610 nm. The absorption at 540 nm corresponds to the π-π* transition of the conjugated backbone in the P3ATs[52,53], while the two peaks at 570 nm to 610 nm are the 0-1 and 0-0 transition whose relative intensity is indicative of an interchain-delocalized excitation resulting from the intermolecular coupling between the polymer chains.[54,55] The absorption peak positions were summarized in **Tables S1**. With branched side chains closer to the polymer backbone, the aggregation behavior becomes more obvious, as indicated by the higher 0-0 transition intensity. After being annealed at 130 °C for 0.5 h, the absorptions of polymers are further red-shifted, therefore, the annealing modified the assemblies of this polymer in the films.

Thermal Properties

The thermal properties of conjugated polymers are critical for determining the kinetics of fluctuations in local structures

due to molecular motions of the polymer chain, such as π–π stacking distances and backbone dihedral angles, which will, in turn, affect charge transport.[56–59] Here, we aim to understand the influence of branch position on the thermal property. Previous work has already shown that by increasing the sidechain length, the T_g of conjugated polymer would decrease.[18,23] However, there is limited work illustrating the effect of the branch location on the thermal property. Furthermore, how the dynamics of the backbone and side chains are mutually affected is still not well understood. Thus, here we compared P3HT with P3(4MP)T and P3(3MP)T by shift the methyl group closer to the polymer backbone.

Therefore, we measured thermal transitions for P3ATs, including backbone glass transitions and melting behaviors, using both DMA and DSC. The results are shown in **Figure 3** and the T_g and T_m for P3ATs are also tabulated in **Table 1**. Due to the limited availability of the polymer sample, it is challenging to perform traditional DMA test with dog-bone bars. Here, we measured the backbone T_g of the P3ATs by using a modified DMA that only requires a small amount of polymer (~10 mg).[46] This was achieved by reinforcing the polymer using woven glass fiber mesh as supporting substrate. **Figure 3A** showed the results for DMA analysis including the T_g of four P3AT polymers. There is almost 50% drop in storage modulus with temperature below backbone T_g (Figure S10), which is due to the β-transition temperature, also known as alkyl side-chain relaxation, depending on the side chain type, having a very low value around −100 to -50 °C.[23] However, the β-transition is not obvious from DMA results except for P3HT, due to perhaps the reinforcing of woven glass fiber mesh as supporting substrate on the polymer. Here, we identified the broad peak for tan δ and E" as the backbone T_g. A noticeable decrease of backbone T_g was observed from 62.4 °C for poly(3-pentylthiophene) (P3PT) to 21.6 °C for P3HT (**Table 1**). Furthermore, the large difference in T_g observed between P3ATs bearing side chains with the same number of carbon (e.g. six carbon) but different isomeric structures are especially interesting. By simply shift the methyl group for one carbon position, the backbone T_g of poly(3-(4-methylpentylthiophene)) (P3(4MP)T) increases by 34 °C, and reached 55.6 °C compared with P3HT. Further shift the branch point closer to backbone chains (poly(3-(4-methylpentylthiophene)) (P3(3MP)T)) leads to an even higher backbone T_g (80.5 °C). Thus, moving the methyl branch by one carbon space on the side chains can tremendously change the T_g of the backbone. Furthermore, the measured T_g results from DSC (Figure 2B) showed the same trend as of DMA measurements, although the exact T_g values are lower due to the different mechanisms of two methods, where DMA measures dynamic signals, while DSC measures thermodynamic signals. It should also be acknowledged that this may be associated with greater uncertainty due to weak step change signal during glass transition across a wide temperature range from the DSC. T_g obtained from the peak of E" is lower than that form the peak in tan δ, however, is shown better agree with DSC.

The interesting observation of different T_g dependence on branch position can be rationalized by different local chain dynamics. **Scheme 3** is a schematic representation of the dynamics of different carbon sites along the side chains for P3ATs. Spheres with different radius were used to represent the spatial range of the motions of different carbon sites along the side chains separately. Studies have shown that the dynamics of the backbone and side chains are mutually affected.[18] The mobility of atoms closer to the backbones is suppressed due to the restriction from the slow motions of stiff backbones, which was suggested by Gomez *et. al* using molecular dynamics simulations and solid-state NMR relaxation measurements.[18] This restrictive effect from the backbones decays along the side chain. And at the branching point, due to the steric hindrance effect, the mobility of atoms may also be restricted. In addition, using quasielastic neutron scattering (QENS), Gomez *et al.* discovered that thiophene backbone motion is enhanced as the side-chain length increases from hexyl to dodecyl,[18] because the faster motion of longer side chains leads to faster backbone dynamics. Compared to linear alkyl chains, branched alkyl chains with the same number of carbon atoms are closer to the main chain. For example, compared to P3(4MP)T, P3(3MP)T could be interpreted as moving the methyl group at the chain end to one carbon atom position closer to the conjugated backbone. Along this line, turning a linear side chain into a branched side chain while fixing the total number of carbons restricts the motion of side chains. Moving the branching position closer to the backbone would further suppress the motion of side chains, due to lower configurational entropy for branched side chains. Consequently, the backbone dynamics are affected.

Besides, the influence of the branched position on the melting behavior of P3ATs was studied. Among the consequences of the changed molecular packing is that the alkyl side-chain structure would affect the melting temperature of P3ATs.[30,31,60] We summarized P3AT's melting temperature with respect to their isomeric structures in a table (Table S2). Segalman *et al.* showed that the melting temperature of P3ATs could be tuned by side-chain functionalization.[31] For polymers with similar molecular weights, the main chain melting transitions for P3HT occurs at 234 °C, while when the number of carbon in the alkyl groups increases from 6 to 12, the melting transition decreases from 234 °C to 164 °C. Furthermore, introducing the branched architecture of the 3-(2-ethyl)hexyl side chain was surprisingly shown to depress the main chain melting transition temperature to 71 °C and 83 °C (two distinct peaks). The ethyl group in the side chain could generate great steric hindrance thus resulting in the lower compact packing of molecular chains in the crystalline regions. This was further confirmed by Salleo *et. al*, who proposed that P3EHT exhibits tighter alkyl stacking (≈14.1 Å) and much longer π-π stacking distance (≈ 5.09 Å) as compared to P3HTs.[22] However, we showed that introducing the branched architecture of the side chain could instead increase the melting temperature of P3ATs. The DSC heating curves of P3PT, P3HT, P3(4MP)T, and P3(3MP)T are shown in **Figure 4**, and the key parameters are tabulated in

Table 1. All four P3AT polymers present a single melting peak. Among the four polymers, the melting temperature of P3HT is the lowest (224.9 °C), and turning the linear side chains to branched ones, the melting temperature presents an upward trend (243.8 °C for P3(4MP)T) whereas melting temperature for P3(3MP)T (260.9 °C) is even higher than for P3PT (254.8 °C). The trend of melting behavior agrees with their backbone glass transition temperature for P3ATs as shown in **Figure 7**.

Thin Film Morphology

The high glass transition and melting temperature of P3(4MP)T and P3(3MP)T with respect to P3HT presumably results from their different molecular packing structure. To verify this, GIWAXS experiments for P3ATs were performed. The orientation of P3AT polymer chains in crystallites in three-dimensional directions is schematically shown in **Figure 5**. The distance between polymer backbones in the (a) direction is the lamella distance (d_{lam}) which could be calculated from the (100) Bragg diffraction (d_{100}). π-π stacking is in the (b) direction, the distance between polymer chains in this direction could be obtained from (010) Bragg diffraction. The polymers orientation to the bare silicon substrate and crystalline nature can be obtained from GIWAXS. The 2D GIWAXS images of the films before and after annealing at 130 °C for 1 h are shown in **Figure 6** and the out-of-plane and in-plane 1D GIWAXS profiles are presented in **Figure S11**. Both as-spun and annealed P3AT films showed predominantly edge-on packing, which agrees with previous reports.[22] All P3ATs exhibited semicrystalline structures with strong lamellar stacking and π-π stacking diffractions. Upon annealing, the crystalline structure became more ordered, shown as the increased intensity and reduced full width at half maxima of (h00) and (010) peaks. The fitted peak position and FWHM of the lamellar stacking (100) and the π-π stacking distance (010) are summarized in **Table 2**. First, we discuss the dependence the lamella packing with different side chains. As one would expect, longer side chains result in increased $d_{100.}$ Comparing P3HT with sidechain packing distance of 15.90 Å, the P3PT has significantly smaller packing distance of 14.51 Å, which agrees with the literature.[60,61] The branched side-chain structure also affects d_{100}. Polymers with a closer branching point showed a reduction in d_{100} (15.75 Å for P3(4MP)T, 14.68 Å for P3(3MP)T). Both are lower than that of the P3HT polymer. Second, we discuss the influence on branch point on the π-π stacking distance. There is almost no change in π-π stacking distance when comparing P3PT with P3HT. When the branched point is closer to the polymer backbone, π-π stacking distance increased, due to increased steric hindrance between two adjacent polymer chains. The π-π stacking distance from 3.75 Å to 3.89 Å for P3(4MP)T and P3(3MP)T. The lamellar packing distance showed an opposite trend upon systematically varying the side-chain structure. As shown in **Figure 7**, we noted that backbone T_m shows an inverse trend as d_{100} for P3ATs. It could be the case that higher T_m corresponds to the tighter packing along with side-chain direction. Previous work showed the interlayer stacking distance of the lamellar crystalline structure had an inverse trend as T_m for the random copoly(3-alkylthiophene)s, poly(3-butylthiophene-co-3-octylthiophene).[62]

AFM was performed on both as-cast (**Figure S12**) and thermally annealed polymer films (**Figure 8**) to study the film morphology using tapping mode. All four polymers displayed similar nanofibrillar textures that commonly found for semicrystalline conjugated polymers.

The effect of side-chain branching on charge transport was further examined with the organic field-effect transistors (OFET) (**Figure S13**). We did not observe the trend of charge transport mobilities decreases with increasing π-π stacking distance of the P3AT polymer films with respective to their side-chain structure.

Conclusions

Four P3AT derivatives were synthesized to investigate the influence of the length, shape and branching position of side chains on the thermal transitions and molecular packing of the polymers. Moving the branch point closer to polymer backbone has been shown to increase the backbone T_g and T_m due to further reduction of side-chain motions thus also leads to lower backbone dynamics. Meanwhile, from the point of view of molecular packing, introducing the branched side chains results in a tighter molecular packing. This work provides a new perspective on the correlations between the molecular structure to various properties in conjugated polymers. Furthermore, changing the side-chain branch position can provide a powerful tool to turn the glass transition and melting temperatures of conjugated polymers.

Conflicts of interest

There are no conflicts to declare.

Acknowledgements

This work was supported by the U.S. Department of Energy, Office of Science, Office of Basic Energy Science under award number of DE-SC0019361. The authors thank Peter V. Bonnesen (CNMS) for assistance during the NMR experiment. Part of the research was conducted at the Center for Nanophase Materials Sciences, which is a DOE Office of Science User Facility. L.G acknowledge the financial support from NSF-DGE NRT program #1449999. We also thank Prof. Zhenan Bao for help during OFET device fabrication and test.

References

1 T. Someya, Z. Bao and G. G. Malliaras, *Nature*, 2016, **540**, 379–385.
2 D. J. Lipomi, Z. Bao and G. Editors, *MRS Bull.*, 2017, **42**, 93–97.
3 A. C. Arias, J. D. Mackenzie, I. Mcculloch, J. Rivnay and A. Salleo, *Chem. Rev.*, 2010, **110**, 3–24.

4 M. Kaltenbrunner, M. S. White, E. D. Głowacki, T. Sekitani, T. Someya, N. S. Sariciftci and S. Bauer, *Nat. Commun.*, 2012, **3**, 770.

5 P. Cheng, G. Li, X. Zhan and Y. Yang, *Nat. Photonics*, 2018, **12**, 131–142.

6 Y. Zhang, B. Kan, Y. Sun, Y. Wang, R. Xia, X. Ke, Y.-Q.-Q. Yi, C. Li, H.-L. Yip, X. Wan, Y. Cao and Y. Chen, *Adv. Mater.*, 2018, **30**, 1707508.

7 X. Gong, M. Tong, Y. Xia, W. Cai, J. S. Moon, Y. Cao, G. Yu, C.-L. Shieh, B. Nilsson and A. J. Heeger, *Science (80-.).*, 2009, **325**, 1665–1667.

8 C. Luo, A. K. K. Kyaw, L. A. Perez, S. Patel, M. Wang, B. Grimm, G. C. Bazan, E. J. Kramer and A. J. Heeger, *Nano Lett.*, 2014, **14**, 2764–2771.

9 T. M. Swager, *Macromolecules*, 2017, **50**, 4867–4886.

10 J. Mei and Z. Bao, *Chem. Mater.*, 2014, **26**, 604–615.

11 A. Gumyusenge, X. Zhao, Y. Zhao and J. Mei, *ACS Appl. Mater. Interfaces*, 2018, **10**, 4904–4909.

12 C. Wang, H. Ade, Y. Diao, D. Zhao, A. L. Appleton, Y. Zhou, K. Vandewal, W. Ma, L. Fang, Y. Guo, J. Reinspach, S. C. B. Mannsfeld, A. Salleo, G. I. Koleilat, Z. Bao, J. Mei, T. Kurosawa, Y. Gao and Q. Yan, *Adv. Mater.*, 2014, **26**, 3767–3772.

13 J. Mei, H. C. Wu, Y. Diao, A. Appleton, H. Wang, Y. Zhou, W. Y. Lee, T. Kurosawa, W. C. Chen and Z. Bao, *Adv. Funct. Mater.*, 2015, **25**, 3455–3462.

14 I. Kang, H.-J. Yun, D. S. Chung, S.-K. Kwon and Y.-H. Kim, *J. Am. Chem. Soc.*, 2013, **135**, 14896–14899.

15 C. Lu, W.-Y. Y. Lee, X. Gu, J. Xu, H.-H. H. Chou, H. Yan, Y.-C. C. Chiu, M. He, J. R. Matthews, W. Niu, J. B. H. B.-H. Tok, M. F. Toney, W.-C. C. Chen and Z. Bao, *Adv. Electron. Mater.*, 2017, **3**, 1600311.

16 A. T. Yiu, P. M. Beaujuge, O. P. Lee, C. H. Woo, M. F. Toney and J. M. J. Fréchet, *J. Am. Chem. Soc.*, 2012, **134**, 2180–2185.

17 B. C. Schroeder, T. Kurosawa, T. Fu, Y. C. Chiu, J. Mun, G. J. N. Wang, X. Gu, L. Shaw, J. W. E. Kneller, T. Kreouzis, M. F. Toney and Z. Bao, *Adv. Funct. Mater.*, 2017, **27**, 1–8.

18 P. Zhan, W. Zhang, I. E. Jacobs, D. M. Nisson, R. Xie, A. R. Weissen, R. H. Colby, A. J. Moulé, S. T. Milner, J. K. Maranas and E. D. Gomez, *J. Polym. Sci. Part B Polym. Phys.*, 2018, **56**, 1193–1202.

19 D. H. Kim, A. L. Ayzner, A. L. Appleton, K. Schmidt, J. Mei, M. F. Toney and Z. Bao, *Chem. Mater.*, 2013, **25**, 431–440.

20 Y. Zhou, T. Kurosawa, W. Ma, Y. Guo, L. Fang, K. Vandewal, Y. Diao, C. Wang, Q. Yan, J. Reinspach, J. Mei, A. L. Appleton, G. I. Koleilat, Y. Gao, S. C. B. Mannsfeld, A. Salleo, H. Ade, D. Zhao and Z. Bao, *Adv. Mater.*, 2014, **26**, 3767–3772.

21 C. R. Bridges, M. J. Ford, E. M. Thomas, C. Gomez, G. C. Bazan and R. A. Segalman, *Macromolecules*, 2018, **51**, 8597–8604.

22 S. Himmelberger, D. T. Duong, J. E. Northrup, J. Rivnay, F. P. V. Koch, B. S. Beckingham, N. Stingelin, R. A. Segalman, S. C. B. Mannsfeld and A. Salleo, *Adv. Funct. Mater.*, 2015, **25**, 2616–2624.

23 C. Müller, *Chem. Mater.*, 2015, **27**, 2740–2754.

24 J. Vandenbergh, B. Conings, S. Bertho, J. Kesters, D. Spoltore, S. Esiner, J. Zhao, G. Van Assche, M. M. Wienk, W. Maes, L. Lutsen, B. Van Mele, R. A. J. Janssen, J. Manca and D. J. M. Vanderzande, *Macromolecules*, 2011, **44**, 8470–8478.

25 S. Zhang, M. U. Ocheje, L. Huang, L. Galuska, Z. Cao, S. Luo, Y.-H. Cheng, D. Ehlenberg, R. B. Goodman, D. Zhou, Y. Liu, Y.-C. Chiu, J. D. Azoulay, S. Rondeau-Gagné and X. Gu, *Adv. Electron. Mater.*, 2019, **5**, 1800899.

26 S. Zhang, M. U. Ocheje, S. Luo, D. Ehlenberg, B. Appleby, D. Weller, D. Zhou, S. Rondeau-Gagné and X. Gu, *Macromol. Rapid Commun.*, 2018, **0**, 1800092.

27 S.-A. A. Chen and J.-M. M. Ni, *Macromolecules*, 1992, **25**, 6081–6089.

28 Z. Qian, Z. Cao, L. Galuska, S. Zhang, J. Xu and X. Gu, *Macromol. Chem. Phys.*, 2019, **220**, 1900062.

29 S. Pankaj, E. Hempel and M. Beiner, *Macromolecules*, 2009, **42**, 716–724.

30 V. Causin, C. Marega, A. Marigo, L. Valentini and J. M. Kenny, *Macromolecules*, 2005, **38**, 409–415.

31 V. Ho, B. W. Boudouris and R. A. Segalman, *Macromolecules*, 2010, **43**, 7895–7899.

32 J. C. Bijleveld, A. P. Zoombelt, S. G. J. Mathijssen, M. M. Wienk, M. Turbiez, D. M. de Leeuw and and R. A. J. Janssen, *J. Am. Chem. Soc.*, 2009, **131**, 16616–16617.

33 Y. Li, S. P. Singh and P. Sonar, *Adv. Mater.*, 2010, **22**, 4862–4866.

34 F. Zhang, Y. Hu, T. Schuettfort, C. A. Di, X. Gao, C. R. McNeill, L. Thomsen, S. C. B. Mannsfeld, W. Yuan, H. Sirringhaus and D. Zhu, *J. Am. Chem. Soc.*, 2013, **135**, 2338–2349.

35 H. Chen, Y. Guo, G. Yu, Y. Zhao, J. Zhang, D. Gao, H. Liu and Y. Liu, *Adv. Mater.*, 2012, **24**, 4618–4622.

36 H. N. Tsao, D. M. Cho, I. Park, M. R. Hansen, A. Mavrinskiy, D. Y. Yoon, R. Graf, W. Pisula, H. W. Spiess and K. Müllen, *J. Am. Chem. Soc.*, 2011, **133**, 2605–2612.

37 X. Zhan, Z. Tan, B. Domercq, Z. An, X. Zhang, S. Barlow, Y. Li, D. Zhu, B. Kippelen and S. R. Marder, *J. Am. Chem. Soc.*, 2007, **129**, 7246–7247.

38 X. Guo, F. S. Kim, S. A. Jenekhe and M. D. Watson, *J. Am. Chem. Soc.*, 2009, **131**, 7206–7207.

39 T. Lei, J. H. Dou and J. Pei, *Adv. Mater.*, 2012, **24**, 6457–6461.

40 R. Miyakoshi, A. Yokoyama and T. Yokozawa, *Macromol. Rapid Commun.*, 2004, **25**, 1663–1666.

41 M. C. Iovu, E. E. Sheina, R. R. Gil and R. D. McCullough, *Macromolecules*, 2005, **38**, 8649–8656.

42 N. Masuda, S. Tanba, A. Sugie, D. Monguchi, N. Koumura, K. Hara and A. Mori, *Org. Lett.*, 2009, **11**, 2297–2300.

43 S. Tamba, S. Tanaka, Y. Okubo, H. Meguro, S. Okamoto and A. Mori, *Chem. Lett.*, 2011, **40**, 398–399.

44 S. Tamba, K. Shono, A. Sugie and A. Mori, *J. Am. Chem. Soc.*, 2011, **133**, 9700–9703.

45 S. Tanaka, S. Tamba, D. Tanaka, A. Sugie and A. Mori, *J. Am. Chem. Soc.*, 2011, **133**, 16734–16737.

46 A. Sharma, X. Pan, J. A. Campbell, M. R. Andersson and D. A. Lewis, *Macromolecules*, 2017, **50**, 3347–3354.

47 S. D. Oosterhout, V. Savikhin, J. Zhang, Y. Zhang, M. A. Burgers, S. R. Marder, G. C. Bazan and M. F. Toney, *Chem. Mater.*, 2017, **29**, 3062–3069.
48 B. McCulloch, V. Ho, M. Hoarfrost, C. Stanley, C. Do, W. T. Heller and R. A. Segalman, *Macromolecules*, 2013, **46**, 1899–1907.
49 W. Schilling and H. Kippenberg, *Synth. Met.*, 1989, **28**, 99–104.
50 J. P. Aime, F. Bargain, M. Schott, H. Eckhardt, G. G. Miller and R. L. Elsenbaumer, *Phys. Rev. Lett.*, 1989, **62**, 55–58.
51 W. D. Hong, C. N. Lam, Y. Wang, Y. He, L. E. Sánchez-Díaz, C. Do and W. R. Chen, *Phys. Chem. Chem. Phys.*, 2019, **21**, 7745–7749.
52 B. K. Kuila and A. K. Nandi, *J. Phys. Chem. B*, 2006, **110**, 1621–1631.
53 B. R. D. Mccullough, *Adv. Mater.*, 1998, 93–116.
54 O. Ingana, I. Lundstro, N. Gadegaard and R. Österbacka, *Science (80-.).*, 2000, **287**, 839–842.
55 P. J. Brown, D. S. Thomas, A. Köhler, J. S. Wilson, J. S. Kim, C. M. Ramsdale, H. Sirringhaus and R. H. Friend, *Phys. Rev. B - Condens. Matter Mater. Phys.*, 2003, **67**, 1–16.
56 J. Colmenero, A. Alegra, J. M. Alberdi, F. Alvarez and B. Frick, *Phys. Rev. B*, 1991, **44**, 7321–7329.
57 A. Babel and S. A. Jenekhe, *Synth. Met.*, 2005, **148**, 169–173.
58 K. Vakhshouri and E. D. Gomez, *Macromol. Rapid Commun.*, 2012, **33**, 2133–2137.
59 T. Liu and A. Troisi, *Adv. Funct. Mater.*, 2014, **24**, 925–933.
60 P. T. Wu, H. Xin, F. S. Kim, G. Ren and S. A. Jenekhe, *Macromolecules*, 2009, **42**, 8817–8826.
61 T. A. Chen, X. Wu and R. D. Rieke, *J. Am. Chem. Soc.*, 1995, **117**, 233–244.
62 P. T. Wu, G. Ren and S. A. Jenekhe, *Macromolecules*, 2010, **43**, 3306–3313.

ARTICLE

Table 1. Number averaged molecular weight (M_n), dispersity (Đ), glass transition temperature, and melting temperature of P3AT polymers.

Polymer	M_n (kg/mol)	Đ	Regioregularity (%)	T_g (°C) tan δ	T_g (°C) E"	T_g (°C) DSC	T_m (°C) DSC	Δ H_m J/g
P3PT	22.4	1.12	98	62.4	19.5	26.0	252.8	23.1
P3HT	20.0	1.05	97	21.6	4.4	16.3	233.5	21.1
P3(4MP)T	20.9	1.06	97	55.6	16.7	35.9	253.5	26.2
P3(3MP)T	17.3	1.68	98	80.5	52.7	41.4	261.6	26.3

Table 2. Crystallographic parameters for P3AT polymers.

Polymer		Out of plane		In plane	
		Lamellar spacing (Å)	Lamellar peak FWHM ($Å^{-1}$)	π-π stacking distances (Å)	π-π peak FWHM ($Å^{-1}$)
P3PT	As cast	14.47	0.0700	3.72	0.1472
	Annealed	14.51	0.0576	3.71	0.1227
P3HT	As cast	15.88	0.0610	3.72	0.1369
	Annealed	15.90	0.0505	3.70	0.1154
P3(4MP)T	As cast	15.74	0.0611	3.74	0.1575
	Annealed	15.74	0.0484	3.75	0.1304
P3(3MP)T	As cast	14.78	0.0699	3.88	0.1960
	Annealed	14.69	0.0537	3.89	0.1511

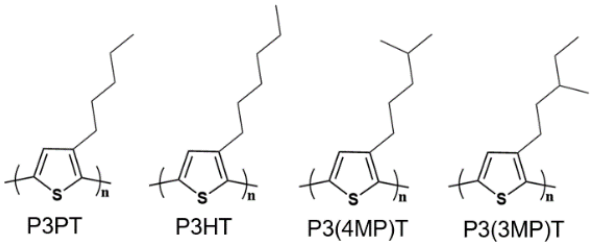

Scheme 1. Chemical structures of poly (3-alkylthiophene-2,5-diyl) derivatives.

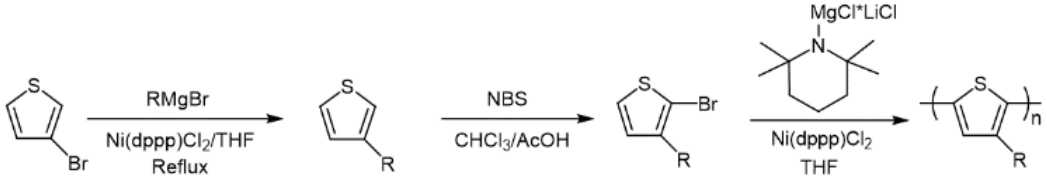

Scheme 2. Synthetic route of poly (3-alkylthiophene-2, 5-diyl) derivatives.

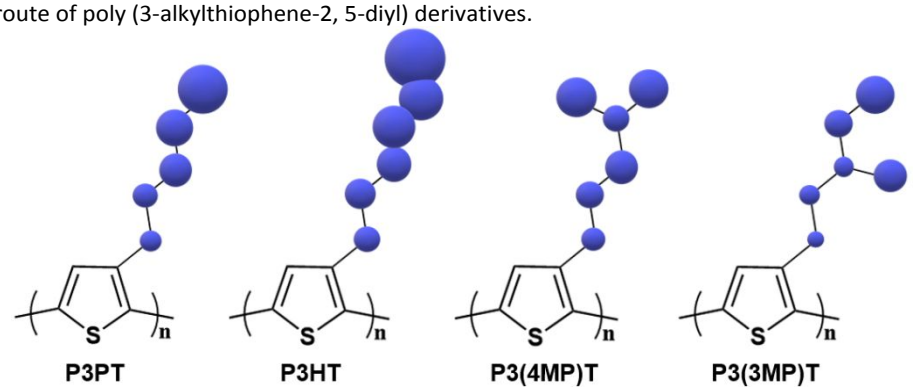

Scheme 3. Schematic for diffusion model of side chains of poly (3-alkylthiophene-2, 5-diyl) derivatives. A sphere is assigned to each carbon site.

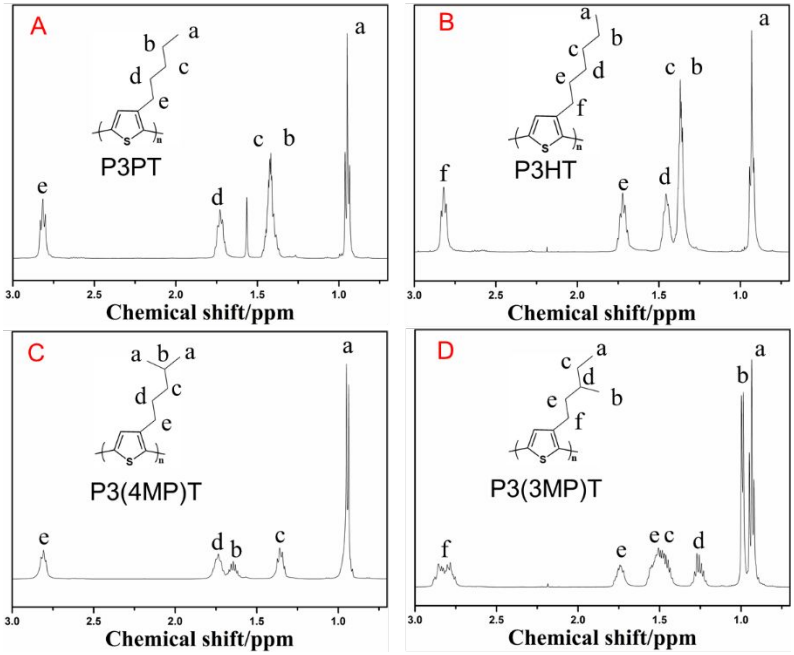

Figure 1. ^{1}H-NMR spectrum of poly (3-alkylthiophene-2,5-diyl) derivatives. (A) P3PT, (B) P3HT, (C) P3(4MP)T, (D) P3(3MP)T.

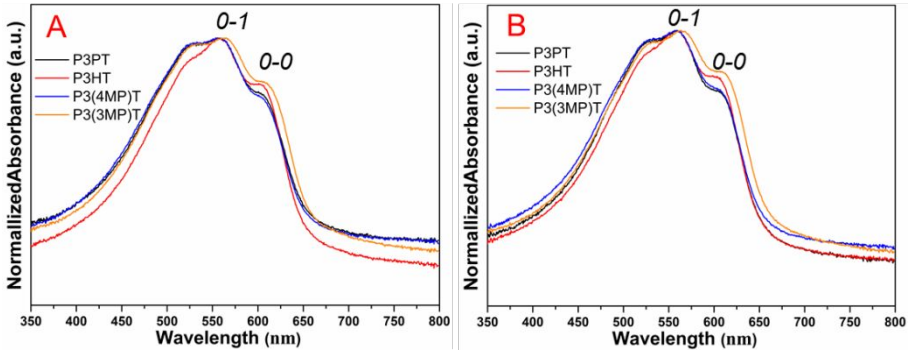

Figure 2. Absorption spectra of polymers films before annealing (A) and after (B) annealing at 130 °C for 0.5 h.

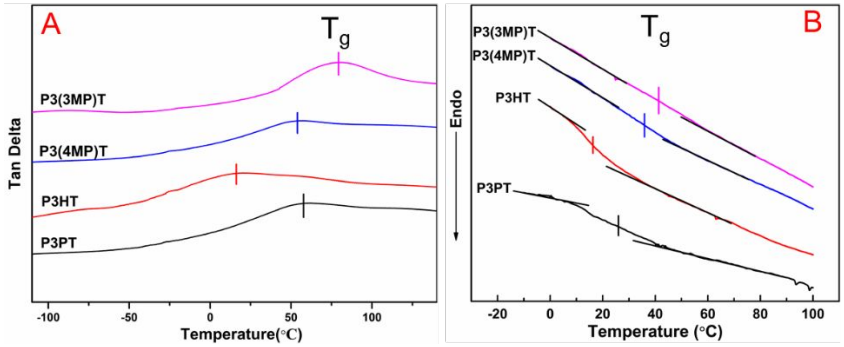

Figure 3. The glass transition phenomenon for various P3ATs. Summary of A) tan δ curve and B) DSC thermograph for P3AT derivatives with their glass transition region highlighted.

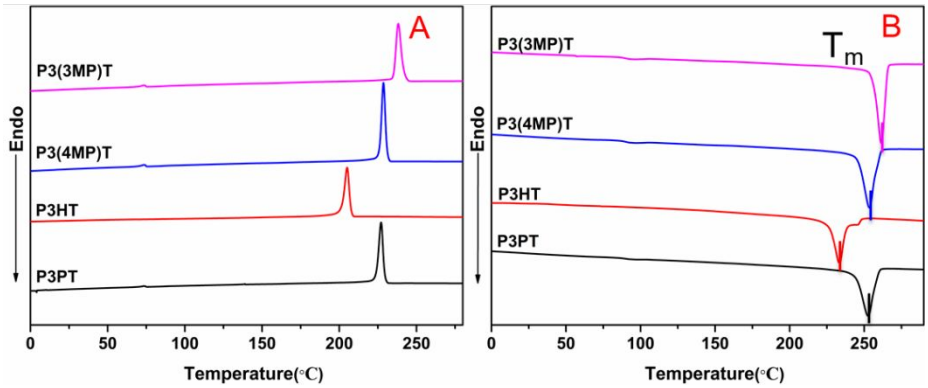

Figure 4. The crystallization (A) and melting (B) behaviour for various P3ATs.

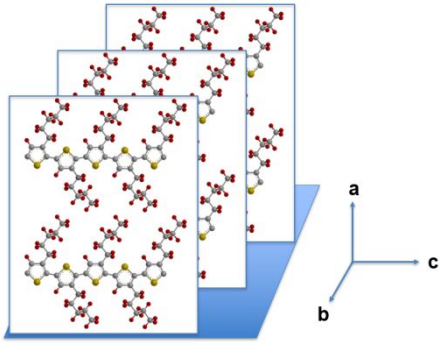

Figure 5. Schematic drawing for the packing structure of P3ATderivatives.

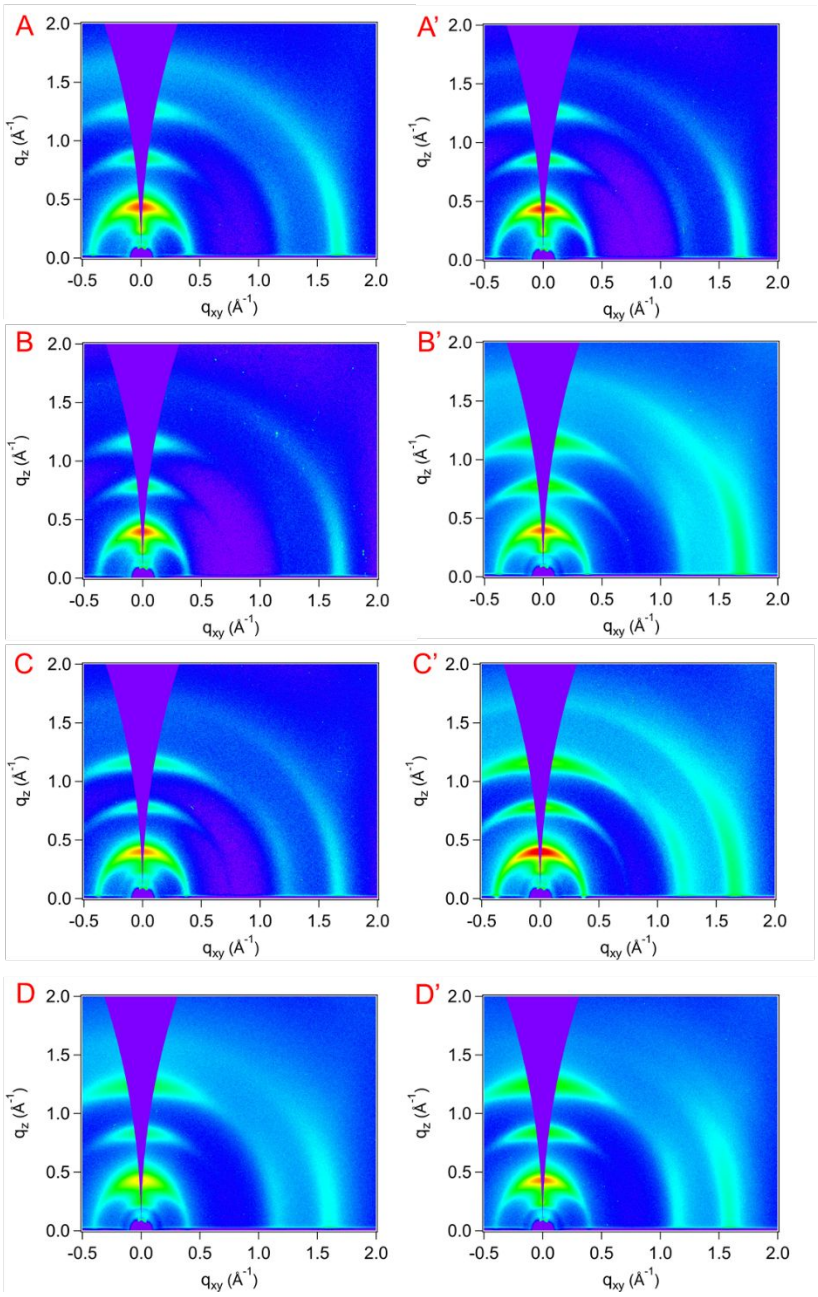

Figure 6. 2D GIWAXS images of P3AT films before (A) P3PT, (B) P3HT, (C) P3(4MP)T, (D) P3(3MP)T and after (A') P3PT, (B') P3HT, (C') P3(4MP)T, (D') P3(3MP)T annealing. 1-D scattering profiles are provided in the supporting information.

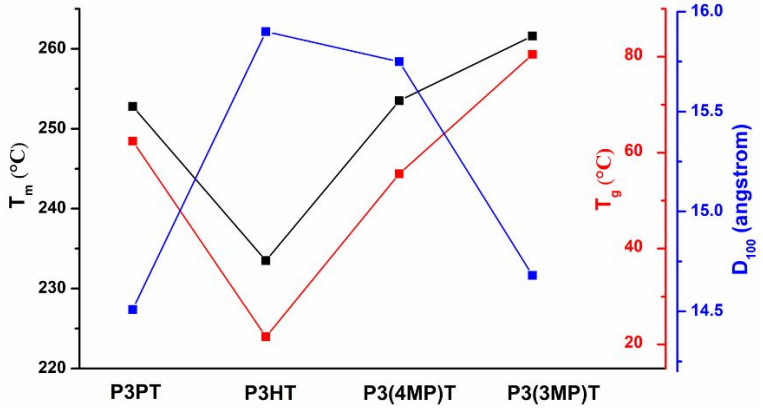

Figure 7. T_m, T_g, and alkyl chain packing distance for various P3ATs .

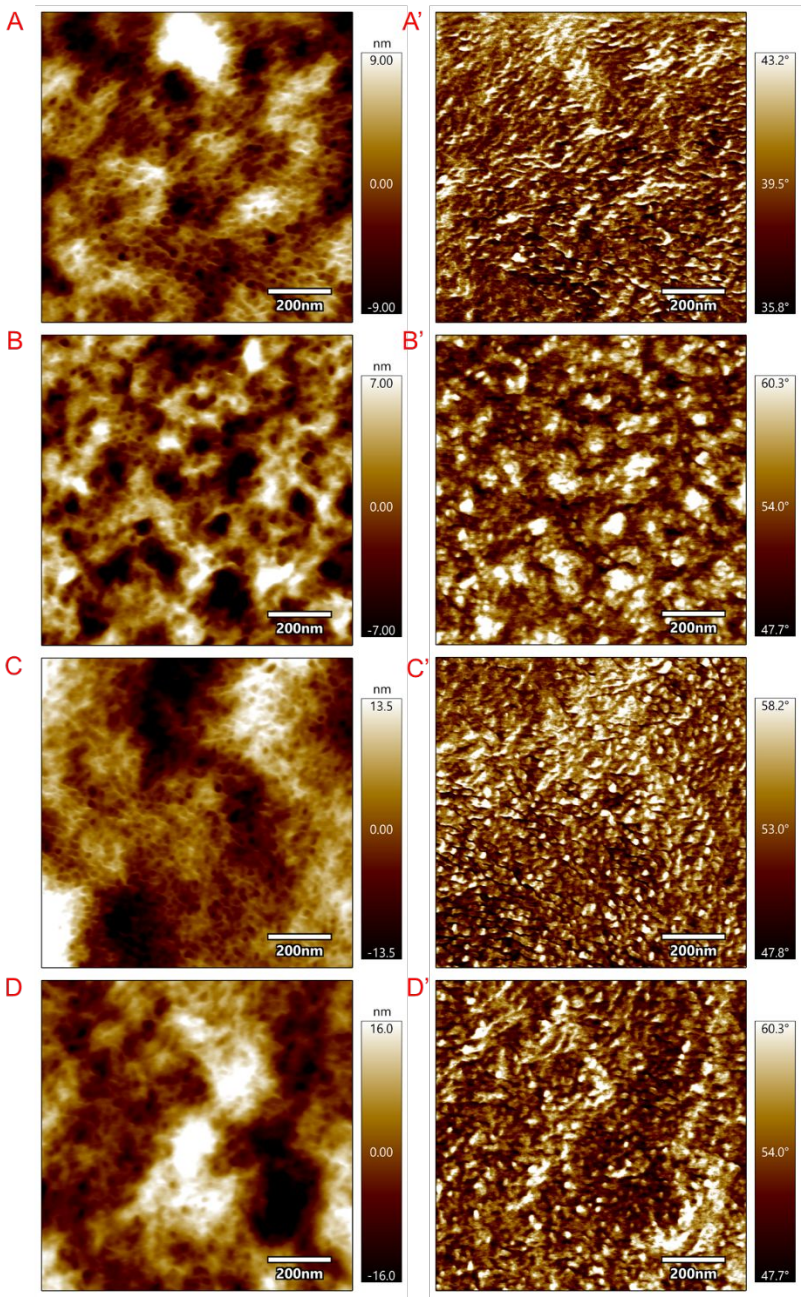

Figure 8. AFM images for thermally annealed P3AT films. A,A') P3PT polymer B,B') P3HT polymer C,C') P3(4MP)T polymer D,D') P3(3MP)T. (A, B, C, D) are height images, (A', B', C', D') are phase images.

Table of Contents

The Role of Side-chain Branch Position on Thermal Property of Poly-3-alkylthiophenes

Zhiqiang Cao, Luke Galuska, Zhiyuan Qian, Song Zhang, Lifeng Huang, Nathaniel Prine, Tianyu Li, Youjun He, Kunlun Hong,* and Xiaodan Gu*

Branching closer to the backbone causes tighter packing in side-chain direction and lower side chains and backbone dynamics. The smaller spacing between adjacent chains decreases the free volume of the polymer system and subsequently increases the T_g.